Electrodeposition of Bi Thin Films on n-GaAs(111)B. Part I: Correlation between the Overpotential and the Nucleation Process.

Alicia Prados, Rocío Ranchal*

Department Física de Materiales, Universidad Complutense de Madrid, 28040, Madrid, Spain,

ABSTRACT

Bismuth thin films constitute a promising nanostructure for the fabrication of spin-based devices. To achieve this goal, it is necessary to obtain high-quality Bi layers with controlled and reproducible properties. Therefore, studies focused on the understanding of the nucleation process and the correlation between the growth conditions and the film properties are of great interest. In this work, we have studied the electrodeposition of Bi thin films onto GaAs(111)B substrates at different overpotentials. In Part I, we have analyzed the nucleation of the films by means of potentiostatic curves. The current density transients have been deconvoluted into individual processes taking into account the energy band diagram of the semiconductor-electrolyte interface. The deconvolution of the current density transients indicates that Bi electrodeposition follows a 3D nucleation controlled by diffusion, accompanied by concurrent processes such as both proton adsorption and reduction. The competition of these processes is controlled by the energy distribution of the surface states at the semiconductor-electrolyte interface and determines the nucleation process. The correlation between the properties of the Bi films and the Bi/GaAs interface with the nucleation process, i.e., with overpotential, is discussed in detail in Part II of this work.

Introduction

Bismuth (Bi) is a semimetal with interesting electronic properties arising from a carrier mean free path[1,2] and a Fermi wavelength[3,4] larger than those obtained in other materials. These two characteristics make Bi a suitable scenario for the study of classical and quantum size effects (SE and QSE) on the electronic properties[5-9]. In addition, Bi surface states are strongly spin-polarized via the Rashba effect[10], which could cause Bi to have a strong impact in spintronics.[11] Although there are some studies about these effects on Bi nanowires,[12, 13] thin films represent a better configuration to study the implementation of these effects in Bi-based devices. In fact, very recently a large spin to charge conversion induced by spin-orbit coupling in a Bi/Ag Rashba interface has been measured.[14]

Compared to other growth techniques, the electrodeposition presents some advantages for the deposition of Bi films. First, this technique has a high deposition rate, and it is compatible with patterning and large-scale production. Second, high quality Bi thin films can be obtained onto metals (Au, Cu, Al)[15-18], semiconducting substrates (GaAs)[19-21], glassy carbon[22] and fluorine-doped tin oxide (FTO)-coated glass[23]. Among all these possible substrates, semiconductors appear as the most interesting for a better integration of Bi films in electronic devices. Rectifying[20] or tunnel[21] Schottky barriers can be obtained by varying the substrate doping level, leading to different mechanisms for electron transport through the interface, Thermionic Emission or Thermionic-Field Emission. Moreover, just modifying the substrate surface orientation it is possible to synthesize Bi thin films with both a different crystalline texture and interfacial electrical properties[21]. Therefore, a wide range of devices could be fabricated starting from just one material and growth technique.

In our previous work we reported some of the electrochemical properties of n-GaAs electrodes[24, 25] and proved that they are suitable to grow high quality Bi thin films[21]. In this work

we study the correlation between the growth overpotential and the nucleation process of 40 nm Bi layers grown by dc electrodeposition. We have chosen five different growth potentials within the range that goes from Bi(III) reduction until water reduction potential: -0.15 V, -0.2 V, -0.3 V, -0.5 V and -0.7 V (measured with respect to the Ag/AgCl electrode). We have employed highly doped GaAs substrates since tunnel Schottky junctions are a promising structure for spin injection/detection[26]. We have chosen the (111)B orientation since it provides Bi films with a slightly better morphology and higher out-of-plane crystal quality than those obtained onto GaAs(110)[21]. In Part I of this work we study the effect of the overpotential on the nucleation process that is dependent on the kinetics of Bi(III) ion reduction and on the onset of concurrent processes such as H^+ reduction or ion adsorption, e. g., H^+ or OH^-, which play an important role in the overall process[27]. We have analyzed the current density transients obtained during the nucleation process by a procedure developed by Palomar-Pardavé *et al.*[28] that allows the deconvolution of the overall current into its individual contributions[29-32]. In the literature there are several works that report the use of this formalism to study the nucleation of metallic deposits onto metallic surfaces[28, 31-36]. However, to our best knowledge, there are rather few works in which this procedure has been used to analyze the nucleation of metallic films onto semiconducting surfaces[37, 38]. In view of our results we can conclude that the nucleation process is directly related to the distribution of states in the energy band diagram of the semiconductor-electrolyte interface (SEI). In Part II of this work we correlate the morphological and structural properties of the Bi films as well as the electrical properties of the Bi/n-GaAs interface with the nucleation process. Therefore, we can conclude that by means of the nucleation process it is possible to control the properties of the layers.

Methods

Electrochemical experiments have been carried out using a stable water-based electrolyte containing 1 mM Bi_2O_3 (bismuth oxide) as the Bi(III) cation source and 1 M $HClO_4$ (perchloric acid) as supporting electrolyte. Solutions were prepared with analytical grade chemicals and deionized water in order to avoid free ions. Bismuth oxide was first added to perchloric acid in a volumetric flask, and then, the solution was made to the mark with deionized water. The pH of the solution (approximately 0.1) was not necessary to be further adjusted. Working electrodes were Si doped n-type GaAs(111)B wafers, supplied by Geo Semiconductors, with a carrier concentration of $(0.9 - 2.4) \cdot 10^{18}$ cm^{-3}. Ohmic contacts were made on the back of the wafers by thermal evaporation of 80 nm of AuGe (2% Ge) and 250 nm of Au, followed by an annealing at 380 ^{o}C in forming gas for 90 s. The total surface area exposed to the electrolyte was 0.15 cm^2 in all cases. Prior to each experiment, substrates were degreased and then etched to remove GaAs native oxide under darkness conditions. First, substrates are dipped in a solution of HCl (10% vol.) for 2 minutes to remove arsenic and gallium oxides[39]. Then, substrates are rinsed in deionized water for 2 minutes to remove Ga-Cl_x species since they are soluble in water[40]. Finally, substrates are immersed in 1 M $HClO_4$ (supporting electrolyte) for 2 minutes to remove possible Cl^- ions remaining in the solution or adsorbed at the substrate surface. Then, the substrate surface is protected from air with a drop of 1 M $HClO_4$ (supporting electrolyte) when transferred to the Bi(III) solution, where substrates remained 2 minutes to reach a stable open circuit potential (OCP). In this condition, the substrate surface is oxide-free with about one monolayer coverage of elementary As[39]. The nucleation and growth of the Bi layers were performed in a three-electrode cell with a platinum mesh as counter electrode and a Ag/AgCl (3 M NaCl) reference electrode supplied by BASi ($E_{ref} \approx 0.196$ V vs SHE). In this study, all potentials are referred to this electrode. Electrochemical experiments were

controlled by a PalmSens EmStat3+Blue potentiostat. After deposition, films were rinsed in deionized water and dried with N_2.

Results and Discussion

1. *Cyclic Voltammetry and Current Density Transients*

Figure 1.a shows a cyclic voltammetry (CV) of two scans performed on the n-GaAs substrate in the Bi(III) solution. From this CV we can extract some information about our system (the n-GaAs/electrolyte junction) and the Bi(III)/Bi redox couple. The equilibrium potential of the junction is the open circuit potential, OCP = 100 mV. As will be seen later it is useful to define the overpotential of the junction as the bias voltage applied to it, i.e., the potential applied to the n-GaAs substrate (E) measured with respect to the equilibrium potential, $\eta_{SEI} = E - OCP$. The equilibrium potential of the Bi(III)/Bi redox couple ($E_{Bi,eq}$), that is the second crossover of the CV at null current, is different from the OCP, approximately 10 mV. This equilibrium potential is referred to the deposition of Bi(III) ions onto a metallic Bi surface. However, when the substrate surface is different from metallic Bi, an extra energy is needed to reduce the Bi(III) ions on it, i.e., create bonds between the Bi atoms and the surface atoms of the substrate. This extra energy is called the nucleation overpotential, $\eta_{Bi,nucelation} = E_{Bi,onset} - E_{Bi,eq}$. The onset potential of Bi reduction ($E_{Bi,onset}$) on the n-GaAs substrate, that is the intersection between the rise current and the CV baseline, is higher in scan 1 (≈-150 mV) than in scan 2 (≈-100 mV) and consequently, $\eta_{Bi,nucelation}$ is higher in scan 1 (≈-160 mV) than in scan 2 (≈-110 mV). This difference between onset potentials is a reflection of the surface blockade produced by a layer of adsorbed hydrogen (H_{ads}) as we reported in previous works[24, 25]. Finally, since we are going to study the nucleation of Bi(III) ions onto a n-GaAs substrate, we define the overpotential of Bi (η_{Bi}) as the applied potential (E) measured with

respect to the onset potential, $\eta_{Bi} = E - E_{Bi,onset}$. It should be considered the onset potential of scan 2 since it is related to an n-GaAs surface without H_{ads} blockade.

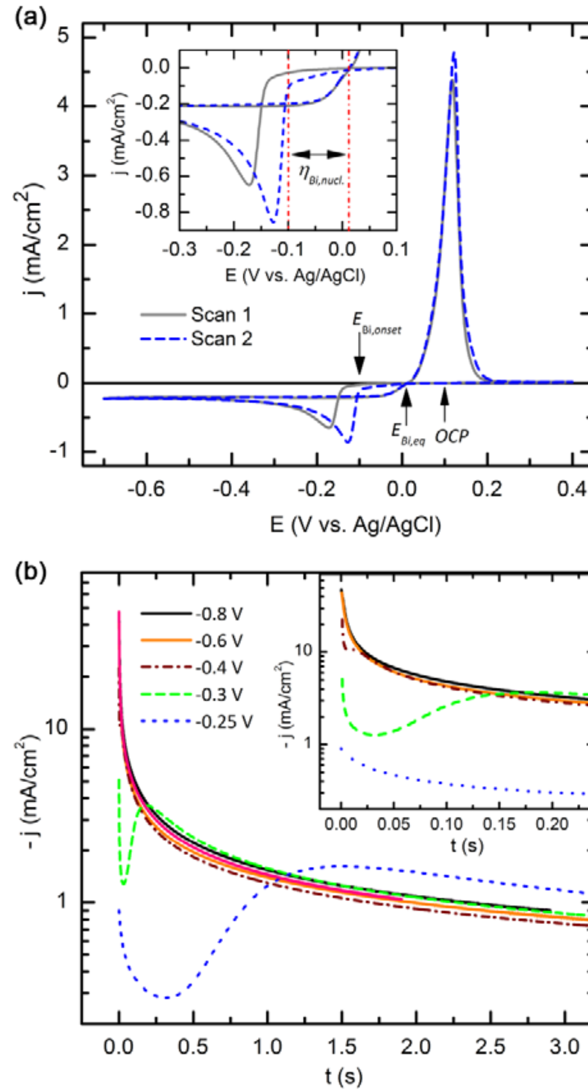

Figure 1. (a) Cyclic voltammetry scans performed at 10 mV/s on the GaAs(111)B substrate in the 2 mM Bi(III) solution. The inset shows an enlargement of the reduction peaks. (b) Current density transients for Bi nucleation on n-GaAs (111)B substrates at different η_{SEI}.

In order to analyze the effect of η_{SEI} on the nucleation of the Bi layers it is necessary to unblock the GaAs surface, eliminating the H_{ads} layer. To do so, we have carried out a growth

procedure that consists of the scan route described in ref. 25 in which a first CV is performed to unblock the n-GaAs surface (Figure 1.a) and then a dc potential is applied to grow the Bi film. By this procedure, the properties of the electrodeposited Bi layer as well as the Bi/GaAs(111)B interface will only be dependent on η_{SEI}. Figure 1.b shows the current density transients obtained during the nucleation of Bi films onto n-GaAs(111)B substrates at five different cathodic potentials: -0.15 V, -0.2 V, -0.3 V, -0.5 V and -0.7 V. To make clear the presentation and discussion of the following results, we will use the equivalent overpotentials ($\eta_{SEI} = E - OCP$): -0.25 V, -0.3 V, -0.4 V, -0.6 V and -0.8 V. The transients obtained at low η_{SEI} (from -0.25 V to -0.3 V) exhibit an initial decay of the current that cannot be explained either by the Cottrell equation ($j \sim t^{-1/2}$) or an exponential decay ($j \sim e^{-kt}$). Therefore, this is not a diffusion-controlled process as it does not apply to the former, and neither can be associated with a pure charging of the SEI[30] as it cannot be explained by the latter. After this decay, the current rises due to the formation and growth of three-dimensional (3D) Bi nuclei, reaching a maximum (j_{max}, t_{max}) that corresponds to the overlap of the diffusion fields of the growing nuclei. Then, the current decreases and tends to a constant value as the electrode surface evolves from the 3D to a 2D geometry due to the overlap of the Bi nuclei. The transients obtained at higher η_{SEI} (-0.6 V and -0.8 V) only show a monotonic current decay that tends to a constant value at longer time.

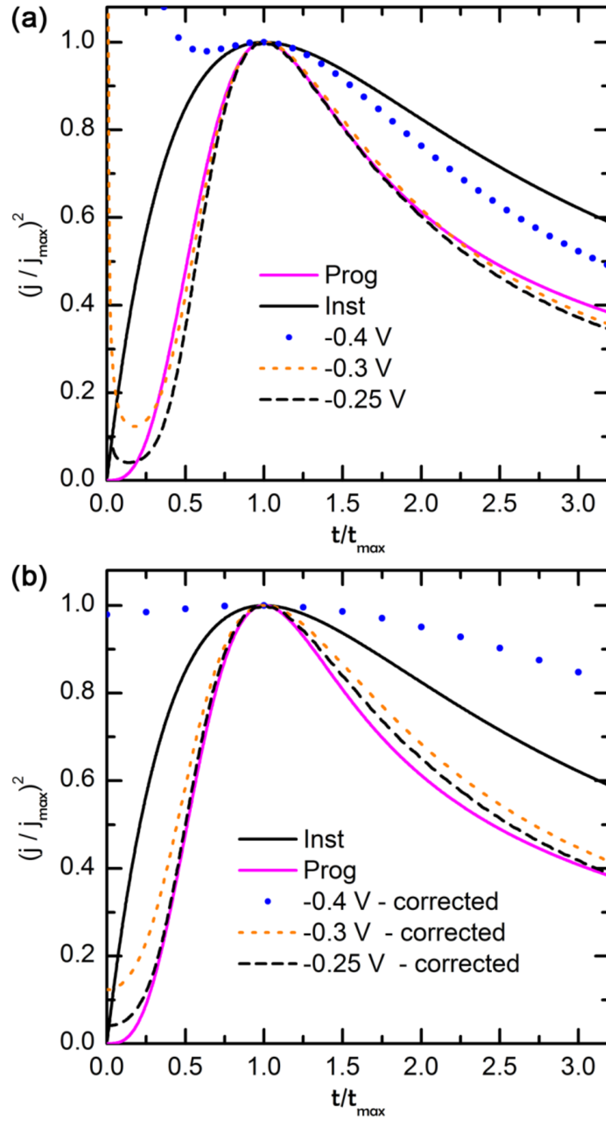

Figure 2. Nondimensional plots of theoretical curves for instantaneous and progressive nucleation and current density transients obtained at η_{SEI} = -0.25 V, -0.3 V and -0.4 V, (a) as measured and (b) corrected to neglect the initial current decay.

If we try to normalize the current density transients that present a current maximum according to the model derived by Scharifker and Hills[41], it can be seen that the experimental data for η_{SEI} = -0.25 V and -0.3 V lie beyond the theoretical curve for progressive nucleation and the

data obtained for η_{SEI} = -0.4 V do not follow any of the theoretical curves at short times (Figure 2.a). If the curves are corrected according to Rigano *et al.*[42] and the initial current decay is neglected, the normalized curves still differ from the theoretical curves (Figure 2.b). This behavior indicates that the current involved in the nucleation of the Bi films is formed by more than one contribution, which means that the reduction of Bi(III) ion takes place with concurrent processes. This is not surprising if we consider all the different energy states present in the SEI (Figure 3.a).

2. *Energy Band Diagram of the Semiconductor-Electrolyte Interface*

In order to understand the evolution of the Bi films nucleation as a function of η_{SEI} and to elucidate the contributions to the overall current, it is previously necessary to describe the energy band diagram of the studied SEI. It is widely known that semiconductor electrodes are more complex than metal electrodes due to the particular electronic structure of the former. Besides the conduction (CB) and valence bands (VB), which introduce two possible paths for electron transfer, the semiconductor surface has surface states that strongly influence the kinetics of chemical and electrochemical processes that occur on the electrode surface[43, 44]. Surface states can be classified into intrinsic and extrinsic[27, 45]. The former are surface states with short relaxation times ($\tau = 10^{-6}$-10^{-3} s), associated with dangling bonds present at the ideal surface ("truncated bulk"), i.e. only dependent on the crystallographic orientation of the surface[44, 45]. Due to the 2D symmetry of the surface, the dangling bonds give rise to surface bands located in the energy band gap of the semiconductor that can partially overlap with the CB or the VB depending on the charge character of the dangling bond. Extrinsic surface states are assigned to surface imperfections, i.e. perturbations of the ideal surface. The extrinsic states do not have symmetry and consequently, they lead to discrete energy states in the band gap. They have longer relaxation times (τ = 1 s) and predominate over the intrinsic states[44]. In the case of GaAs(111)B, the intrinsic states are related to

the dangling bonds of the surface As atoms. These unsaturated bonds have a donor character and can be considered as half-filled due to the breaking of the covalent bond. Therefore, the As-derived surface band is located near the edge of the valence band and is half-filled[45] (SS_{int} in Figure 3.a). On the other hand, a common extrinsic state on As-rich GaAs surfaces is an As antisite (As atoms in Ga positions each of them surrounded by four As atoms), which produces an acceptor level at 0.75 eV and a donor level at 0.52 eV above the edge of the VB, according to the Advanced Unified Defects Model[45, 46] (SS_{ext} in Figure 3.a).

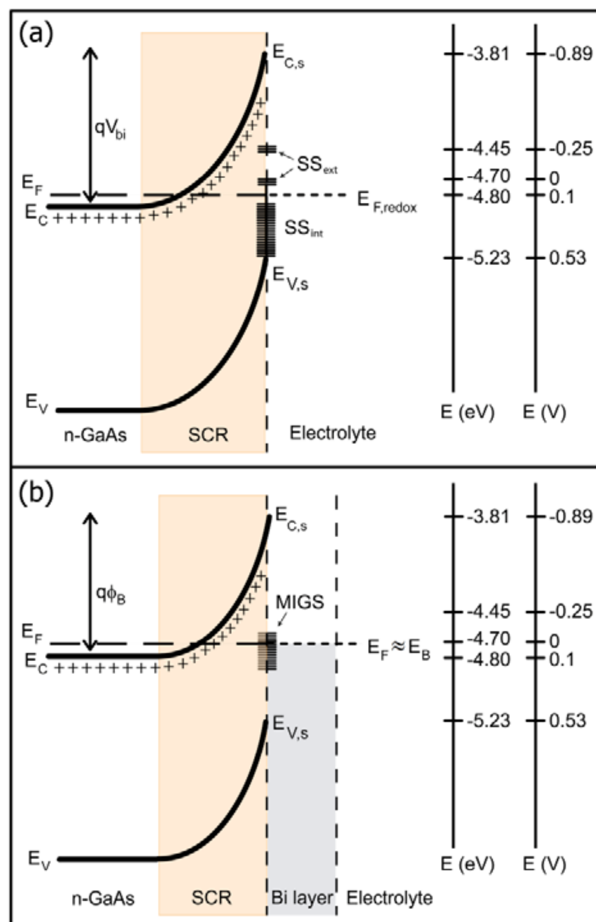

Figure 3. Energy band diagram at OCP conditions of a SEI formed by the Bi(III) solution and (a) an n-GaAs substrate ($n = 2.4 \cdot 10^{18}$ cm^{-3}) and (b) the same n-GaAs substrate covered by a Bi layer. The ionized donors have been represented with crosses (+) to show qualitatively the relation

between the SCR width and the amount of ionized donors contained in it. The energy scale is referred to the vacuum level whereas the potential scale is referred to the Ag/AgCl reference electrode ($E_{Ag/AgCl}$ = 0.196 V vs SHE).

Although the SEI can be a more complex structure, it is possible to establish some analogies with a Schottky barrier where the metal role is played by the electrolyte and the interfacial states are the surface states of the GaAs electrode (Figure 3.a)[43, 44, 47]. When an electrode is immersed into an electrolyte, the system reaches the electrochemical equilibrium by leveling the Fermi energy levels of both media transferring charge from one to another[43, 47]. For an n-GaAs electrode, the electrons are transferred from the semiconductor to the electrolyte, leaving a space charge region (SCR) with a fixed positive charge associated with the ionized donors of the semiconductor. Since the electrons cannot be free in the electrolyte, they remain at the semiconductor surface, occupying surface states. Some of these electrons interact with chemical species present in the electrolyte producing adsorbed species at the semiconductor surface. This adsorption saturates the dangling bonds and minimizes the surface energy, avoiding reconstruction or relaxation of the semiconductor surface[44]. In our case, some of the transferred electrons strongly interact with the cations of the electrolyte through the dangling bonds of As surface atoms which could be considered perpendicular to the semiconductor surface and half filled[45]. Since the predominant cations are protons, As-H bonds are created[45]. These bonds have already been observed by photoelectron spectroscopy on GaAs surfaces treated with HCl and rinsed in water[39]. However, As-OH bonds have not been observed except when the surface is treated with a basic solution as NH_4OH and rinsed in water[48]. Therefore, we can suppose that the GaAs surface is mainly covered by As-H bonds and the amount of As-OH bonds is very small. Due to the covalent nature of the As-H bonds[49, 50], a highly stable adsorbed hydrogen (H_{ads}) is formed on the GaAs surface[24]. This blockade is reflected as a shift between the

cathodic peaks of consecutive scans of a CV performed on an n-GaAs substrate in the Bi(III) solution[24] (Figure 1.a). In the first scan, the As-H bonds are substituted by As-Bi bonds during the cathodic stage and by As-OH bonds during the anodic stage[25, 50]. When the CV ends at the OCP, the GaAs surface will be mainly covered by OH^-, ClO_4^- and water molecules due to the electrostatic attraction produced by the ionized donors present in the SCR of the GaAs[47, 50, 51]. These species are not strongly attached to the GaAs surface and do not block it. Therefore, just after performing a CV the n-GaAs surface is momentarily unblocked[25].

The flat-band potential of an n-GaAs electrode immersed in 1 M $HClO_4$ is $U_{fb} \approx$ -0.81 V vs Ag/AgCl[52]. This potential indicates the position of the SEI Fermi level at flat band conditions, E_F^{fb}. If we consider the energy level of the Ag/AgCl reference electrode referenced to the vacuum level (E_{ref}= -4.7 eV[43]), we can obtain E_F^{fb} as follows:

$$E_F^{fb} = E_{ref} + qU_{fb} \approx -3.89eV \quad (1)$$

where q is the electron charge. From E_F^{fb} we can obtain the position of the CB edge at the surface as follows:

$$E_{C,s} = E_F^{fb} - k_B T \cdot \ln\left(\frac{n}{N_C}\right) \approx -3.81eV \quad (2)$$

where n is the electron concentration of the electrode ($\approx 2 \cdot 10^{16}$ cm^{-3} [52]), Nc is the effective density of states in the CB of the GaAs ($4.7 \cdot 10^{17}$ cm^{-3})[51], k_B is the Boltzmann constant and T is the temperature. The position of the VB edge at the surface can be obtained as follows:

$$E_{V,s} = E_{C,s} - E_g = -5.23eV \quad (3)$$

where E_g = 1.42 eV is the band gap of GaAs[51]. The position of the Fermi level at equilibrium is provided by the OCP = 0.1 V vs Ag/AgCl, which is equivalent to -4.8 eV with respect to the vacuum level. This position approximately coincides with that obtained by

photocapacitance spectroscopy for the higher surface states associated with surface unsaturated bonds (E_1 = $E_{C,s}$ - 0.98 eV)[53]. This indicates that at OCP conditions surface dangling bonds are saturated by adsorbed species and therefore, intrinsic surface states are filled[45]. To reinforce our energy diagram, it should be pointed out that the equilibrium potential for the Bi(III)/Bi redox couple, $E_{Bi,eq}$ = 10 mV, equivalent to -4.71 eV, coincides with the Fermi level of an ideal Bi/n-GaAs junction in equilibrium, which is between 0.5 eV and 0.55 eV above the VB edge according to the model of Metal Induced Gap States (MIGS)[45] (Figure 3.b). The contact potential between the n-GaAs electrode and the Bi(III) solution (V_{bi}) at OCP conditions is:

$$qV_{bi} = E_{C,s} - E_C = \left(E_{C,s} - E_F\right) + (E_F - E_C) \approx 1.1eV \tag{4}$$

where the Fermi energy level at the bulk has been calculated according to Nilsson approximation[54] (E_F - E_C = 90 meV). The width of the space charge region (w) is:

$$w = \sqrt{\left(\frac{2\varepsilon}{q \cdot N_D^+}\right) \cdot \left(V_{bi} - V - \frac{k_B T}{q}\right)} \tag{5}$$

where N_D^+ is the concentration of the ionized donors (equal to the electron concentration), V is the applied bias and ε is the dielectric permittivity of the GaAs[51]. At OCP conditions i.e. without polarization (V = 0), w = 23.4 nm. The positive charge at the SCR associated with the ionized donors is proportional to this width, $Q_{sc} = q \cdot N_D^+ \cdot w$. With all these data, we can depict the energy band diagram of the studied SEI (Figure 3.a-b). Although it is similar to a Schottky junction, it should be pointed out that an electrolyte is more complex than a metal because it has more than one energy level (one per redox couple), and the energy levels are not discrete but present a Gaussian distribution due to the effect of the water molecules (polar molecules) surrounding the ions[43, 44, 55, 56].

3. Analysis of the Current Density Transients

When a η_{SEI} is applied to the n-GaAs/electrolyte junction, the junction is biased and the Fermi level moves away from the equilibrium position (OCP conditions) approximately the same amount translated to the energy scale. This induces a change in the charge of the semiconductor: variation of w, of electron and hole surface populations and of the charge contained in the surfaces states. To maintain the SEI neutrality, the charge at the Helmholtz layer is rearranged by desorption and adsorption processes, as well as reorientation of water molecules and solvated polyatomic anions such as ClO_4^-. If the Fermi level coincides or surpasses the energy level of a redox couple (for example, H^+/H_2), this reaction is activated. Therefore, several processes are expected to contribute to the current density transients recorded during the nucleation of the Bi films.

In order to extract the individual contributions to the overall current, the transients shown in Figure 1.b have been analyzed by a formalism developed by Palomar-Pardavé *et al.*[28]. This formalism consists of the analysis of the transients by a nonlinear fit of the experimental data to different nucleation models, using the Marquardt–Levenberg algorithm, which allows the deconvolution of the total current density ($j(t)$), into individual contributions[29, 31, 32, 36, 57]. For cathodic reactions, where the current density is negative, the absolute value of the current density should be used. Our analysis shows that all transients are indeed formed by several contributions that can be related to different processes that take place at a SEI when it is biased. At low η_{SEI}, two regimes delimited by an induction time (t_0) can be distinguished. During the first regime, $t < t_0$, four different processes run simultaneously:

[a] Charging of the SEI capacitance. The equivalent electrical circuit of the SEI is formed by several capacitances and resistances: semiconductor capacitance (C_{sc}), surface states capacitance (C_{SS}), double layer capacitance (C_H), charge transfer resistance (R_t), etc.[40, 43, 47].

When the SEI is biased, the capacitances are charged. Although it is more complex, we have made the approximation of considering the SEI as a simple series *RC* circuit[47, 58]. Therefore, the current involved in the charging of the SEI capacitance is:

$$j_{SEI}(t) = \frac{Q_{SEI}}{\tau_{SEI}} \cdot \exp\left(-\frac{t}{\tau_{SEI}}\right) \tag{6}$$

where Q_{SEI} is the electrical charge involved in the process, and $\tau_{SEI} = R \cdot C$ its time constant, where *R* is the SEI resistance and *C* the SEI capacitance. The duration of the process can be considered as 5 times τ_{SEI}.

[b] Desorption of ClO_4^- and OH^- anions. As aforementioned, the nucleation of the Bi film starts after a CV that ends at the OCP (Figure 2.a). At this point, the substrate surface will be mainly covered by anions and water molecules adsorbed during the anodic stage of the CV [24, 50]. When the applied potential is varied from the OCP to a more negative potential, the SCR width decreases (eq. 5) as well as the amount of positive fixed charge. Consequently, some of the adsorbed anions are desorbed to maintain the electrical neutrality of the SEI. This process is directly related to the charging of the SEI. This process can be described as follows:

$$j_{des}(t) = \frac{Q_{des}}{\tau_{des}} \cdot \exp\left(-\frac{t}{\tau_{des}}\right) \tag{7}$$

where Q_{des} is the electrical charge involved in the process and τ_{des} its time constant[30].

[c] Adsorption of H^+ on the GaAs surface. This process produces a change of the n-GaAs surface from a hydroxylated (As-OH) to a hydrogenated state (As-H). It occurs via intrinsic and extrinsic surface states, and can take place even when the H^+ reduction reaction is not activated as it has been observed by Electrochemical Impedance Spectroscopy[59]. This process can be described by:

$$j_{ads}(t) = \frac{Q_{ads}}{\tau_{ads}} \cdot \exp\left(-\frac{t}{\tau_{ads}}\right) \tag{8}$$

where Q_{ads} is the electrical charge involved in the process and τ_{ads} its time constant[30].

[d] Reduction of H^+ on the GaAs surface by the reaction:

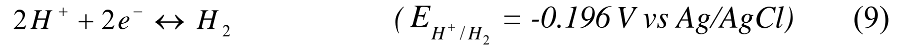

$$2H^+ + 2e^- \leftrightarrow H_2 \qquad (E_{H^+/H_2} = \text{-0.196 V vs Ag/AgCl}) \tag{9}$$

This process follows the Volmer-Heyrovsky route[60], and requires two electrons of the CB, i.e. it occurs through conduction band states[49, 60]. Due to the high electron concentration of the n-GaAs substrates, the SCR is rather narrow and conduction electrons can reach the electrolyte either by thermionic emission over the barrier or by tunneling through it (Thermionic-Field Emission theory, TFE)[61]. The whole process can be described by the following expression[31, 62]:

$$j_{PR} = z_{PR} \cdot F \cdot k_{PR} \tag{10}$$

where z_{PR} is the number of electrons involved in the reduction reaction, F is Faraday's constant and k_{PR} is the rate constant of the reaction.

When the SEI is charged and the Helmholtz layer has been reorganized, the second regime starts for $t > t_0$, and Bi(III) ions start to reduce into metallic Bi progressively covering the GaAs surface. This process is described as follows:

[e] Reduction of Bi(III) ions into metallic Bi following a 3D nucleation controlled by diffusion[29], and delayed by an induction time, t_0, associated with the initial current decay[42, 63]. This process can be described by the following expression:

$$j_{3D}(t) = P_4 \cdot (t - t_0)^{-1/2} \cdot \theta(t - t_0) \tag{11}$$

where $\theta(t)$ is the substrate surface area covered by the diffusion zones of the Bi nuclei[64]:

$$\theta(t) = 1 - \exp\left\{ - P_2 \cdot \left[(t - t_0) - \frac{(1 - \exp[- A \cdot (t - t_0)])}{A} \right] \right\} \tag{12}$$

and

$$P_2 = N_o \cdot \pi \cdot D \cdot \left(\frac{8\pi \cdot c_o M}{\rho} \right)^{1/2} \tag{13}$$

$$P_4 = \left(\frac{z \cdot F \cdot D^{1/2} \cdot c_o}{\pi^{1/2}} \right) \tag{14}$$

where N_o is the density of active sites for nucleation on the GaAs surface, A the Bi(III) ion nucleation rate per active site, D the diffusion coefficient of Bi(III) ions, c_o the concentration of Bi(III) ions in the bulk of the electrolyte, M the molar mass of metallic Bi and ρ the density of metallic Bi. To fulfill the requirement of dimensional homogeneity, c_0 should be introduced in $mol \cdot cm^{-3}$ and ρ in $g \cdot cm^{-3}$.

Similarly to H^+ reduction, Bi(III) ions reduction occurs via conduction band states[65] following the TFE theory. The onset of Bi reduction alters H^+ reduction because of the competition for nucleation sites at the GaAs surface and conduction electrons. Therefore, the component associated with H^+ reduction (j_{PR}) should be modified taking into account the presence of the growing Bi nuclei and their diffusion zones, i.e. $j_{PR} = z_{PR} \cdot F \cdot k_{PR} \cdot [1 - \theta(t)]$. However, the adsorption of H^+ (j_{ads}) is independent of the substrate surface coverage, θ, because adsorption and nucleation processes take place at different surface sites and through different electronic states. Therefore, these processes run in parallel[30, 59]. Consequently, H^+ adsorption takes place until the whole GaAs surface is covered by Bi nuclei. Initially, we also considered the contribution assigned to H^+ reduction on the Bi surface. However, we found that this contribution is negligible due to the slow kinetics of this reaction on this metal since both the adsorption and the charge-transfer step are

rather slow[66, 67]. In fact, Bi is a notoriously poor electrocatalyst for hydrogen evolution reaction[68]. To sum up, the current density transients shown in Figure 1.b have been analyzed by fitting the experimental data to the following expressions:

$$j = j_{SEI} + j_{des} + j_{ads} + j_{PR} \qquad t < t_0 \qquad (15)$$

$$j = j_{ads} + j_{PR} \cdot [1 - \theta(t)] + j_{3D} \qquad t > t_0 \qquad (16)$$

In order to obtain accurate and reliable results, all the experimental current density transients shown in Figure 1.b have been fitted computing the value, the standard error and the lower (LCL) and upper (UCL) 95% confidence limits of the parameters Q_{SEI}, τ_{SEI}, Q_{des}, τ_{des}, t_0, Q_{ads}, τ_{ads}, k_{PR}, D, A and N_0. The best-fit parameters are listed in Table 1, whereas their respective errors obtained on basis of the 95% confidence limits are listed in Table 2. Data listed in Table 1 and Table 2 show that all the best-fit values present relative errors below 10%, except for the parameters Q_{SEI} and τ_{SEI} obtained at η_{SEI} = -0.25 V. The relative errors are significant in this case because of the insufficient resolution for the transient. For more accurate values it would have been necessary to record it with a lower time step than used, t_{step} = 0.01 s. The nucleation rate, A, obtained at η_{SEI} = -0.8 V also presents a relative error higher than 10%. It could be a consequence of the interference produced by the H_2 bubbles as it is explained afterward.

η_{SEI} (V)	-0.25	-0.3	-0.4	-0.6	-0.8
τ_{SEI} (ms)	6.5	0.6	-	-	-
Q_{SEI} ($\cdot\mu C\cdot cm^{-2}$)	1.0	6.3	-	-	-
τ_{des} (ms)	44.0	4.8	-	-	-
Q_{des} ($\mu C\cdot cm^{-2}$)	19	10	-	-	-
t_0 (ms)	454	47	0.8	-	-
τ_{ads} (ms)	2945	483	0.9	2.0	2.9
Q_{ads} ($\mu C\cdot cm^{-2}$)	988	236	35	65	112
k_{PR} ($\cdot 10^{-8}$ $mol\cdot cm^{-2}\cdot s^{-1}$)	-	0.4	5.1	8.5	6.3

D ($\cdot 10^{-5}$ $cm^2 \cdot s^{-1}$)	2.6	2.1	1.6	1.8	2.1
A (s^{-1})	0.3	9.8	163	1993	2997
N_o ($\cdot 10^{6}$ cm^{-2})	5.2	12	38	120	55

Table 1. Best-Fit Parameters Obtained from the Analysis of the Experimental Current Density Transients Shown in Figure 1.b. The Corresponding Errors are Summarized in Table 2. To facilitate their lecture, the numbers have not been rounded according to their errors.

η_{SEI} **(V)**	**-0.25**	**-0.3**	**-0.4**	**-0.6**	**-0.8**
$\Delta\tau_{SEI}$ *(ms)*	1.2	$9.2 \cdot 10^{-3}$	-	-	-
ΔQ_{SEI} *($\cdot 10^{-2}$ $\mu C \cdot cm^{-2}$)*	27	3.9	-	-	-
$\Delta\tau_{des}$ *(ms)*	1.4	$38 \cdot 10^{-3}$	-	-	-
ΔQ_{des} *($\mu C \cdot cm^{-2}$)*	0.29	0.04	-	-	-
Δt_0 *(ms)*	1.1	$77 \cdot 10^{-3}$	$3.9 \cdot 10^{-3}$	-	-
$\Delta\tau_{ads}$ *(ms)*	17	1.5	$3.3 \cdot 10^{-3}$	$20 \cdot 10^{-3}$	$14 \cdot 10^{-3}$
ΔQ_{ads} *($\mu C \cdot cm^{-2}$)*	4.3	0.47	0.044	1.1	0.79
Δk_{PR} ($\cdot 10^{-10}$ $mol \cdot cm^{-2} \cdot s^{-1}$)	-	0.10	0.62	9.7	2.8
ΔD ($\cdot 10^{-9}$ cm^2 s^{-1})	23	3.9	4.1	4.9	9.7
ΔA (s^{-1})	0.023	0.089	3.7	81	376
ΔN_o ($\cdot 10^{5}$ cm^{-2})	3.6	0.73	1.7	17	7.5

Table 2. Standard Error Derived from the Lower (LCL) and Upper (UCL) 95% Confidence Limits of the Best-Fit Parameters Obtained from the Analysis of the Experimental Current Density Transients Shown in Figure 1.b and reported in Table 1.

Figure 4.a-e shows the experimental transients plotted in Figure 1.b, and their individual contributions obtained from the corresponding best-fit parameters listed in Table 1. It can be noted that the formalism developed by Palomar-Pardavé *et al.*[28] accurately describes all the transients, except for the minima of the current density transients obtained at lower η_{SEI} (-0.25 V and -0.3 V). This is probably a consequence of the approximation we made to represent the charging of the SEI as a series *RC* circuit when it is rather more complex. The charging of the SEI (j_{SEI}, red dashed line

in Figure 4.a-b) is detected only at low η_{SEI} (-0.25 V and -0.3 V). As η_{SEI} increases, the charging is faster (τ_{SEI} decreases) and the mobilized charge increases (Q_{SEI} increases). If we considered the energy band diagram of the SEI (Figure 5.a-c), when a cathodic potential is applied, the GaAs Fermi level shifts upward with respect to the electrolyte Fermi level[47], leading to a proportional increase of the electron population at the semiconductor SCR (increase of Q_{SEI}), a decrease of the SCR width (increase of the capacitance of the SEI, C), and a decrease of the electron barrier height, $\phi_n = (V_{bi} - E)$ (Figure 5.a-c), which eventually leads to a decrease of the SEI resistance (R). Since R decreases exponentially with η_{SEI}[43], whereas C increases as the square root[43, 47], $\tau_{SEI} = R{\cdot}C$ decreases when increasing η_{SEI}. Anion desorption (j_{des}, blue dashed line in Figure 4.a-b) also increases with η_{SEI} due to the decrease of the SCR width and, therefore, the decrease of the positive charge associated with the ionized donors (Figure 5.a-c). As a result, a larger amount of ions (Q_{des}) are desorbed to maintain the electrical neutrality of the SEI. The time constant, τ_{des}, decreases up to η_{SEI} = -0.3 V when the process becomes undetectable. As expected, t_0 is higher than τ_{SEI} and τ_{des}, i.e. the reduction of Bi(III) ions does not start until the SEI has been reorganized. As well as τ_{SEI} and τ_{des}, t_0 decreases rapidly with the overpotential as the SEI reorganization is faster. For η_{SEI} higher than -0.4 V, t_0 is smaller than the step time used to record the experimental transients and therefore, it is considered null.

Proton reduction on the GaAs surface (j_{PR}, light blue dashed line in Figure 4.b-e) is activated at η_{SEI} above -0.25 V (Table 1). According to TFE theory, k_{PR}, should approximately exponentially increase. However, at η_{SEI} = -0.4 V k_{PR} increases more than expected probably due to the pinning of the Fermi level at the higher surface states assigned to As antisites (0.75 eV above VB)[44]. The presence of accessible surface states enhances the tunneling of electrons, enhancing the reduction reaction (Figure 5.b). In addition, at η_{SEI} = -0.8 V, k_{PR} slightly decreases coinciding with the onset

of water reduction. This can be associated with the competition between H^+ and water molecules for the GaAs surface sites.

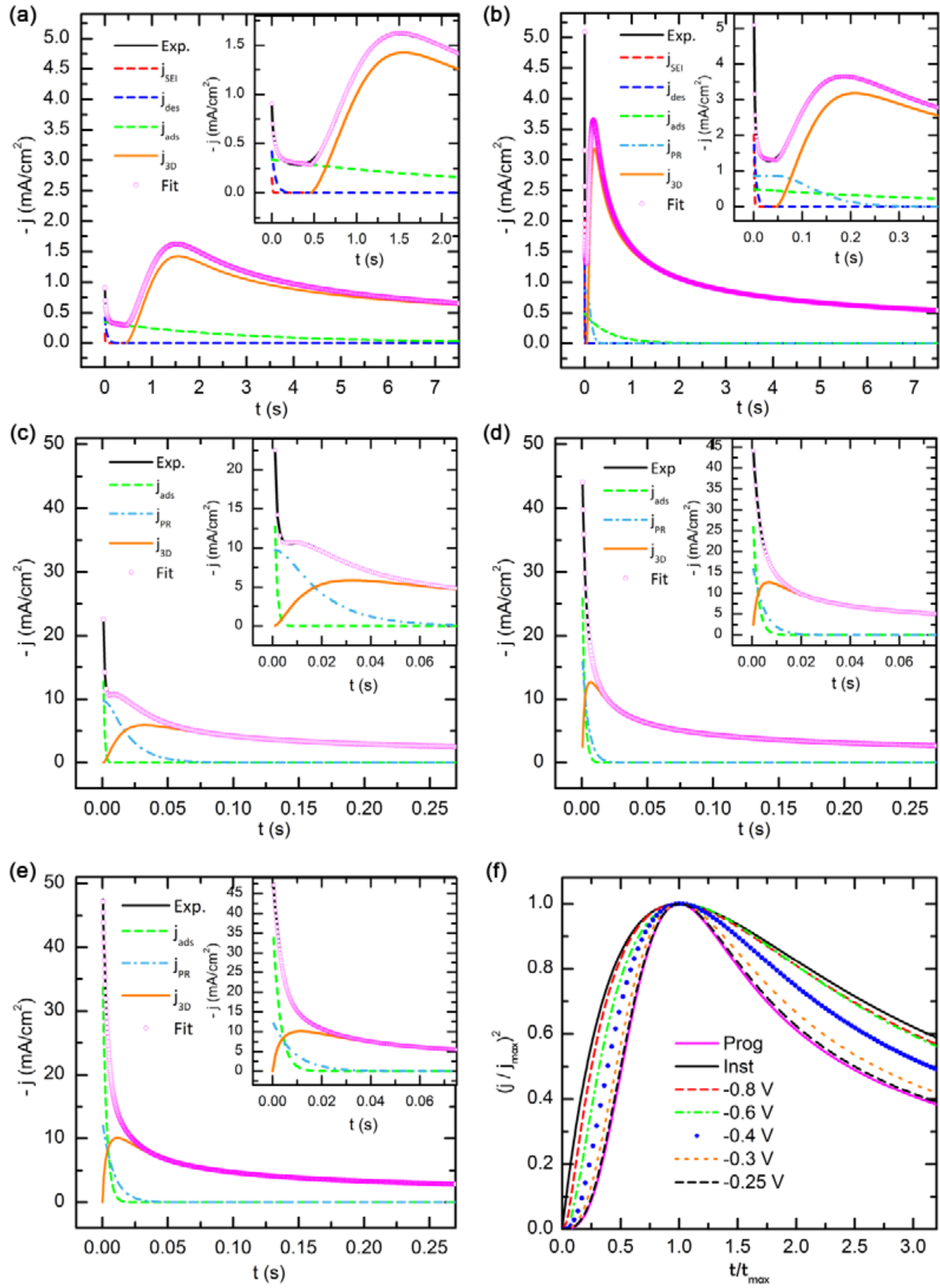

Figure 4. Individual contributions obtained from the deconvolution of the transients recorded at different η_{SEI}: (a) -0.25 V, (b) -0.3 V, (c) -0.4 V, (d) -0.6 V, and (e) -0.8 V. (f) Nondimensional plots of j_{3D} contribution (orange line) shown in (a)-(e) and theoretical curves for instantaneous and progressive nucleation.

Bi(III) ion reduction (j_{3D}, orange line in Figure 4.a-e) is activated at η_{SEI} = -0.25 V and is enhanced with η_{SEI}. The nucleation rate of Bi(III) ions, A, shows an approximately exponential dependence with η_{SEI} as expected from the TFE theory. A similar tendency has been reported in other studies[32, 33, 36, 62]. Based on the classical theory of electrocrystallization, Sebastián *et al.*[69] derived an expression for the nucleation rate in terms of the Bi overpotential, $\eta_{Bi} = E\text{-}E_{Bi,onset}$:

$$A(\eta_{Bi}) = \frac{j_0 \cdot \upsilon_a}{z \cdot q}\left(\frac{2\sigma}{k_B T}\right)^{1/2} \cdot \exp\left(\frac{\alpha \cdot z \cdot q}{k_B T}\eta_{Bi}\right) \cdot \exp\left(-\frac{8\pi\sigma^3\upsilon_a^2}{3 \cdot z^2 \cdot q^2 \cdot k_B T \cdot \eta_{Bi}^2}\right) \qquad (17)$$

where j_0 is the exchange current density ($A \cdot cm^{-2}$), υ_a is the atomic volume of Bi ($3.5 \cdot 10^{-23}$ cm^{-3}), z is the number of electrons involved in the reduction reaction (3), q is the electron charge ($1.6 \cdot 10^{-19}$ C), σ is the surface tension ($J \cdot cm^{-2}$), k_B is the Boltzmann constant ($1.38 \cdot 10^{-23}$ $J \cdot K^{-1}$), T is the temperature (300 K), α is the transfer coefficient (dimensionless) and η_{Bi} is the overpotential for Bi reduction (in V). This expression considers a contact angle of 90° between the Bi nuclei and the GaAs surface. As done in references (69) and (70), we have fitted the experimental data ($ln(A)$ vs η_{Bi}) according to eq. 17. The best-fit parameters for j_0, α and σ have been obtained excluding the value of A obtained at η_{SEI} = -0.8 V (Table 3). At this overpotential, coinciding with the onset of water reduction, A decreases similarly to k_{PR}, probably due to the competition between Bi(III) ions and water molecules for the GaAs surface sites. The high value obtained for j_0 could be related to the narrow SCR at the SEI which allows charge transfer by tunneling even at low overpotentials. In addition, it could indicate a high affinity between As and

Bi atoms to create bonds, probably as a result of their similar electronic configuration. The low value of α can be produced by the concurrence of H^+ reduction.

The density of active sites, N_o, increases with η_{SEI}, as similarly reported in other studies [32, 33, 36, 62]. At η_{SEI} = -0.8 V, N_o diminishes in spite of the increase of A. A similar feature has been observed in the electrodeposition of cobalt onto glassy carbon, and an explanation based on the formation of H_2 bubbles has been proposed[32]. As the potential becomes more negative, H^+ reduction is enhanced, leading to the formation of H_2 bubbles. These bubbles cover part of the GaAs surface blocking active sites and diminishing N_o. Finally, all the studied transients present values for the diffusion coefficient of Bi(III) ions within (1.6 – 2.6) · 10^{-5} cm^{-2} s^{-1}, which are in the same magnitude of those found in the literature[19, 71]. Once the transients have been deconvoluted, it is possible to represent the j_{3D} contribution in a dimensionless plot according to the theoretical model derived by Scharifker and Hills[41] (Figure 4.f). It can be clearly observed that Bi nucleation is progressive at low η_{SEI} and tends to an instantaneous nucleation as the η_{SEI} is increased. We already reported a progressive nucleation for a η_{SEI} = -0.3 V[21] and attributed it to the competition between Bi(III) ions and H^+ to get adsorbed onto the As surface atoms [25,50]. The same explanation was given by Depestel and Strube to explain the different nucleation mechanism of gold on GaAs(111)A (Ga-terminated surface) and GaAs(111)B surfaces (As-terminated surface)[72]. Thanks to the results reported in this work, we can confirm that the nucleation mechanism of the Bi films is determined by the competition between H^+ adsorption (Q_{ads}) and Bi reduction. At low η_{SEI} , H^+ adsorption is considerably high, whereas the Bi deposition rate is rather low. As η_{SEI} increases, H^+ adsorption diminishes, whereas Bi reduction is enhanced, tending to a mixed nucleation (η_{SEI} = -0.4 V). At higher η_{SEI}, although H^+ reduction slightly increases, the increase of the Bi deposition rate is clearly superior, leading to an instantaneous nucleation.

α (dimensionless)	j_0 (A cm^{-2})	σ ($\cdot\ 10^{-5}$ J cm^{-2})
0.119 ± 0.023	0.0019 ± 0.0014	0.986 ± 0.068

Table 3. Best-Fit Values Obtained from the Dependence of the Nucleation Rate of Bi Reduction (A) with Bi Overpotential (η_{Bi}).

The dependence between H^+ adsorption on the GaAs surface (j_{ads}, green dashed line in Figure 4.a-e) and η_{SEI} is complex because it depends on the concentration of electrons at the surface states, on the Bi deposition rate, and on the concentration of surface holes. The two latter effects are proportional to η_{SEI} but surface states do not have a uniform energy distribution (Figure 3). τ_{ads} is principally related to Bi deposition rate. As the deposition rate increases, the GaAs surface is covered by metallic Bi in less time, and τ_{ads} decreases (Table 1). The dependence of Q_{ads} is more complex because it depends on the three effects above-mentioned. First, if τ_{ads} decreases due to the increase of Bi nucleation rate, a less amount of protons can get adsorbed. Therefore, we should expect a decrease of Q_{ads} with η_{SEI}. However, when η_{SEI} is increased, the Fermi level can surpass empty surface states that become filled and lead to new H_{ads}, which produces an increase of Q_{ads}. Finally, the amount of H_{ads} is affected by the hole population at the surface of the n-GaAs because they can break As-H bonds, leading to unsaturated bonds that tend to adsorb a new proton (increase of Q_{ads}). This last effect is indeed responsible for the higher values of Q_{ads} obtained at certain η_{SEI} in comparison to the charge associated with the formation of one monolayer of H_{ads} , q_m = 232 µC cm^{-2}, even if we considered that two electrons are needed to replace an As-OH bond by an As-H bond[60], and that the atomic surface density of GaAs (111)B is $7.22 \cdot 10^{14}$ cm^{-2}. This seems contradictory with the observations made by Erné *et al.*[60] which show that the GaAs coverage by H_{ads} is of the order of one monolayer. Moreover, it should be taken into account that, as Bi reduction takes place simultaneously, a complete monolayer of As-H cannot be formed. Therefore,

this excess of charge, which cannot be explained by means of surface roughness, suggests that H^+ adsorption is a dynamic process that involves not only adsorption but also desorption steps. The current assigned to this kind of process can be described mathematically by the model developed by Barradas and Bosco[73] which considers several layers of adsorbate, each one with its particular constant rate for adsorption ($\vec{k}_i$) and desorption ($\overleftarrow{k}_i$):

$$I(t) = q_m \cdot \psi_1 \cdot \chi_1 \cdot \exp(-\chi_1 \cdot t) + q_m \cdot \frac{\psi_1 \cdot \chi_1 \cdot \psi_2 \cdot \chi_2}{\chi_1 - \overleftarrow{k}_2} \cdot \left[\exp\left(-\overleftarrow{k}_2 \cdot t\right) - \exp(-\chi_1 \cdot t)\right] \quad (18)$$

where

$$\chi_i = \vec{k}_i + \overleftarrow{k}_i \quad (19)$$

$$\psi_i = \frac{\vec{k}_i}{\chi_i} \quad (20)$$

We suggest that H^+ adsorption is a dynamic process influenced by surface holes. To represent this process we can consider two submonolayers of adsorbed protons with different stability. The first submonolayer is formed by stable As-H bonds produced by the interaction between As dangling bonds with two electrons and the H^+ of the electrolyte[74]. The adsorption rate can be considered high ($\vec{k}_1$>>) due to the strong interaction, whereas the desorption rate can be considered negligible ($\overleftarrow{k}_1 \approx 0$) due to the covalent nature of the As-H bond[49]. The second submonolayer is formed by As-H bonds partially broken by surface holes[74], i.e. dangling bonds partially occupied by holes. Therefore, we can consider that the adsorption rate of this submonolayer is lower ($\vec{k}_2 < \vec{k}_1$) and that the desorption rate is significant ($\overleftarrow{k}_2$>>). If we introduced these conditions in eq. (18):

$$I(t) = q_m \cdot \vec{k}_1 \cdot \exp\left(-\vec{k}_1 \cdot t\right) + q_m \cdot \frac{\vec{k}_1 \cdot \vec{k}_2}{\vec{k}_1 - \overleftarrow{k}_2} \cdot \left[\exp\left(-\overleftarrow{k}_2 \cdot t\right) - \exp\left(-\vec{k}_1 \cdot t\right)\right] \quad (21)$$

and if we consider $\vec{k}_1 < \overleftarrow{k}_2$, we can make the approximations $\exp\left(-\overleftarrow{k}_2 \cdot t\right) - \exp\left(-\vec{k}_1 \cdot t\right) \approx -\exp\left(-\vec{k}_1 \cdot t\right)$ and $\vec{k}_1 - \overleftarrow{k}_2 \approx -\overleftarrow{k}_2$. Therefore, we obtain:

$$I(t) = \left[q_m \cdot \vec{k}_1 \cdot \left(1 + \frac{\vec{k}_2}{\overleftarrow{k}_2} \right) \right] \cdot \exp\left(-\vec{k}_1 \cdot t\right) \tag{22}$$

where $\vec{k}_1 = \left(\tau_{ads}\right)^{-1}$ and $q_m \cdot \left(1 + \frac{\vec{k}_2}{\overleftarrow{k}_2} \right) = Q_{ads}$ in eq. (8). It can be seen that $Q_{ads} > q_m$, in agreement with the best-fit values obtained for this parameter (Table 1). Taking into account these three effects, we can eventually explain the evolution of j_{ads} with η_{SEI} (Figure 4.a-e). At low η_{SEI} (-0.25 V to -0.4 V), τ_{ads} progressively decreases as the Bi nucleation rate increases (Table 1). Since the amount of occupied surface states remains the same (As-derived band and the lower As antisite level), Q_{ads} decreases due to the decrease of τ_{ads} but also due to the decrease of surface hole population (Table 1). If there is no H^+ desorption, Q_{ads} tends to q_m. Accordingly to eq. 21, this occurs when $\vec{k}_1 - \overleftarrow{k}_2 >> \vec{k}_2$ which principally occurs when the desorption rate becomes negligible due to the absence of holes ($\overleftarrow{k}_2 \to 0$) since $\vec{k}_1 > \vec{k}_2$ can still be considered. At η_{SEI} = -0.4 V, although the Fermi level surpasses the higher energy level of the As antisites (0.75 eV above the VB) and they become filled, H^+ adsorption is not enhanced (Q_{ads} does not increase). It should be noticed that this surface level lies above the energy level of Bi(III) ions and H^+ reduction reactions. Since the potential barrier for the electrons is considerably high (eq. 4) but the SCR is considerably narrow (eq. 5) and the two reactions occur via conduction electrons, electron transport will follow the TFE theory[61]. If some surface states are available, as As antisites, they assist the electrons tunneling through the barrier (blue arrows in Figure 5.b). Therefore, the As antisite higher level is set aside to assist both the reduction of Bi(III) ions and H^+ and does not have influence on the H^+

adsorption, i.e. it can be considered that it does not exist. At higher η_{SEI} (-0.6 V and -0.8 V) both reduction reactions become progressively governed by thermionic emission over the barrier (yellow arrows in Figure 5.c), and this extrinsic surface state can be again occupied again by $H_{ads,}$ which progressively increases Q_{ads} (Table 1).

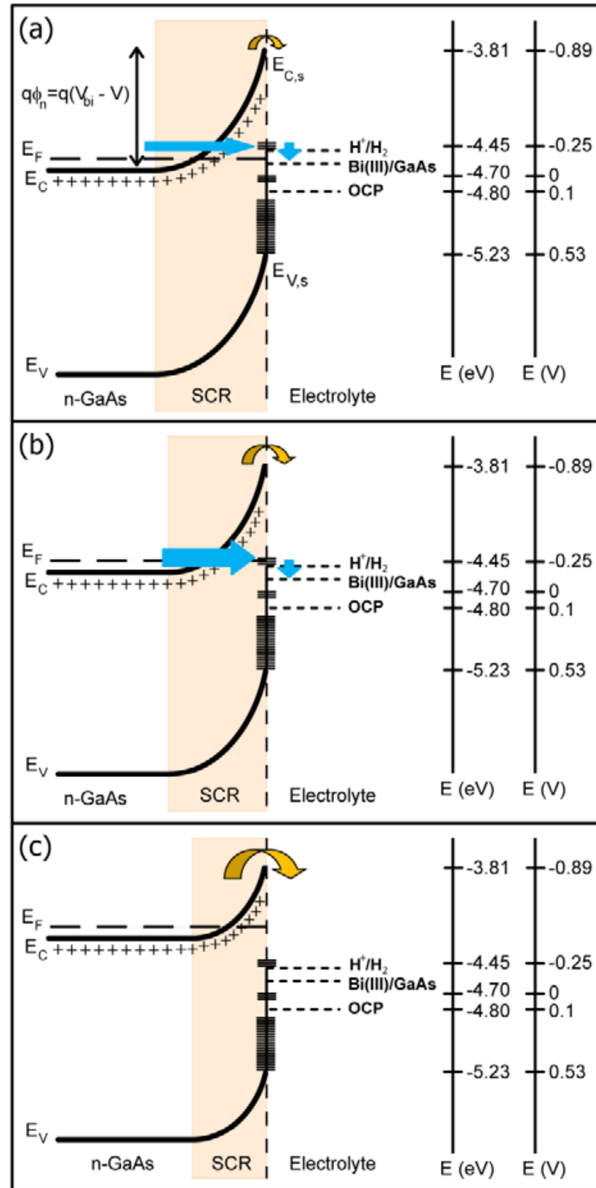

Figure 5. Energy band diagram of the SEI formed by an n-GaAs substrate and the Bi(III) solution at different η_{SEI} (a) -0.25 V, (b) -0.4 V and (c) -0.6 V. The arrows represent the electrons involved

in reduction reactions that are transferred via tunneling and assisted by extrinsic surface states (blue arrows) and via Thermionic Emission (yellow arrow).

Although the energy band diagram of the SEI (Figure 1) assists in the interpretation of the nucleation process of the Bi films and its evolution with the SEI overpotential, some effects have not been considered. On the other hand, the energy distribution of surface states can be altered during the nucleation process due to ion adsorption or to the formation of chemical bonds[27]. Consequently, some states disappear whereas new states called adsorbate-induced gap states (AIGS) or metal-induced gap states (MIGS) are formed. Due to the complexity of these effects, we do not consider them in our model.

Conclusions

In this work we report the influence of η_{SEI} on the nucleation process of 40 nm-thick Bi layers electrodeposited on n-GaAs(111)B substrates. The deconvolution of the current density transients recorded during the nucleation of the layers has proved to be a powerful tool to gain insight into this initial stage of the growth and to determine the processes that are involved in it. In the case of Bi, the reduction of Bi(III) ions occurs simultaneously to H^+ adsorption and reduction. Consequently, the nucleation of the Bi films is conditioned by the competition of these three processes, each one evolving differently with η_{SEI}. On basis of our results, we can conclude that the nucleation of the Bi films is clearly correlated to the energy band diagram of the SEI. The evolution of the different contributions can be rather complex due to the nonuniform distribution of surface states. The nucleation starts with the charging of the semiconductor capacitances and the rearrangement of the Helmholtz layer. As part of this last process, H^+ adsorption and reduction on the GaAs surface can take place. Afterward, Bi reduction starts and alters other processes like H^+ reduction or adsorption. In the first case, the two processes compete for the GaAs surface sites and

the conduction band electrons. In the second case, the Bi reduction indirectly diminishes the H^+ adsorption by progressively covering the GaAs surface because H^+ does not tend to get adsorbed onto metallic Bi.

AUTHOR INFORMATION

Corresponding Author

*a.prados@ucm.es

Phone: (+34) 91 394 4496; Fax: (+34) 91 394 4547

Author Contributions

The manuscript was written through contributions of all authors. All authors have given approval to the final version of the manuscript.

Acknowledgments

This work has been financially supported through project MAT2015-66888-C3-3-R of the Spanish Ministry of Economy and Competitiveness (MINECO/FEDER) and through the project PR26/16-3B-2 of Santander and Universidad Complutense de Madrid. We would like to acknowledge the postdoctoral fellowship granted by Comunidad de Madrid and the European Union (PEJD-2016/IND-2233). We also acknowledge the use of facilities of Instituto de Sistemas Optoelectrónicos y Microelectrónica (ISOM).

References

1. Smith, G. E.; Baraff, G. A.; Rowell, J. M. Effective g Factor of Electrons and Holes in Bismuth. *Phys. Rev.* **1964**, *135*, A1118-1124.

2. Murata, M.; Nakamura, D.; Hasegawa, Y.; Komine, T.; Taguchi, T.; Nakamura, S.; Jaworski, C. M.; Jovovic, V.; Heremans, J. Mean Free Path Limitation of Thermoelectric Properties of Bismuth Nanowire. *J. App. Phys.* **2009**, *105*, 113706.

3. Smith, G. Anomalous Skin Effect in Bismuth. *Phys. Rev.* **1959**, *115*, 1561-1568.

4. Reneker, R. New Oscillatory Absorption of Ultrasonic Waves in Bismuth in a Magnetic Field. *Phys. Rev. Lett.* **1958**, *1*, 440-442.

5. Hirahara, T.; Miyamoto, K.; Kimura, A.; Niinuma, Y.; Bihlmayer, G.; Chulkov, E. V.; Nagao, T.; Matsuda, I.; Qiao, S.; Shimada, K.; et al. Origin of the Surface-State Band-Splitting in Ultrathin Bi Films: from Rasbha Effect to a Parity Effect. *New J. Phys.* **2008**, *10*, 083038.

6. Wada, M.; Murakami, S.; Freimuth, F.; Bihlmayer, G. Localized Edge States in Two-Dimensional Topological Insulators: Ultrathin Bi Films. *Phys. Rev. B* **2011**, *83*, 121310(R).

7. Yang, F. Y.; Lui, K.; Hong, K.; Reich, D. H.; Searson, P. C.; Chien, C. L.; Leprince-Wang, Y.; Yu-Zhang, K.; Han, K. Shubnikov-de Haas Oscillations in Electrodeposited Single-Crystal Bismuth Films. *Phys. Rev. B* **2000**, *61*, 6631-6636.

8. Hoffman, C. A.; Meyer, J. R.; Bartoli, F. J.; Di Venere, A.; Yi, X. J.; Hou, C. L.; Wang, H. C.; Ketterson, J. B.; Wong, G. K. Semimetal-to-Semiconductor Transition in Bismuth Thin Films. *Phys. Rev. B* **1993**, *48*, 11431-11434.

9. Sangiao, S.; Michalik, J. M.; Casado, L.; Martínez-Velarte, M. C.; Morellón, L.; Ibarra M. R.; De Teresa, J. M. Conductance Steps in Electromigrated Bi Nanoconstrictions. *Phys. Chem. Chem. Phys.* **2013**, *15,* 5132-5139.

10. Hirahara, T.; Miyamoto, K.; Matsuda, I.; Kadono, T.; Kimura, A.; Nagao, T.; Bihlmayer, G.; Chulkov, E. V.; Qiao, S.; Shimada, K.; et al. Direct Observation of Spin Splitting in Bismuth Surface States. *Phys. Rev. B* **2007**, *76*, 153305.

11. Khvalkovskiy, A. V.; Cros, V.; Apalkov, D.; Nikitin, V.; Krounbi, M.; Zvezdin, K. A.; Anane, A.; Grollier, J.; Fert, A. Matching Domain Wall Configuration and Spin-Orbit Torques for Efficient Domain-Wall Motion. *Phys. Rev. B* **2013**, *87*, 020402(R).

12. Liu, K.; Chien, C. L.; Searson, P. C. Finite-Size Effects in Bismuth Nanowires. *Phys. Rev. B* **1998**, *58*, R14681-R14684.

13. Cornelius, T. W.; Toimil-Molares, M. E.; Karim, S.; Neumann, R. Oscillations of Electrical Conductivity in Single Bismuth Nanowires. *Phys. Rev. B* **2008**, *77*, 125425.

14. Rojas Sánchez, J. C.; Vila, L.; Desfonds, G.; Gambarelli, S.; Attane, J. P.; De Teresa, J. M.; Magén, C.; Fert, A. Spin-to-Charge Conversion Using Rashba Coupling at the Interface Between Non-Magnetic Materials. *Nat. Commun.* **2013**, *4*, 2944.

15. Yang, F. Y.; Liu, K.; Hong, K.; Reich, D. H.; Searson, P. C.; Chien, C. L. Large Magnetoresistance of Electrodeposited Single-Crystal Bismuth Thin Films. *Science* **1999**, *284*, 1335-1337.

16. Stafford, G. R.; Bertocci, U. In Situ Stress and Nanogravimetric Measurements During Underpotential Deposition of Bismuth on (111)-Textured Au. *J. Phys. Chem. B* **2006**, *110*, 15493-15498.

17. Sandnes, E.; Williams, M. E.; Bertocci, U.; Vaudin, M. D.; Stafford, G. R. Electrodeposition of Bismuth From Nitric Acid Electrolyte. *Electrochim. Acta* **2007**, *52*, 6221–6228.

18. Tishkevich, D. I.; Grabchikov, S. S.; Tsybulskaya, L. S.; Shendyukov, V. S.; Perevoznikov, S. S.; Trukhanov, S. V.; Trukhanova, E. L.; Trukhanov, A. V.; Vinnik, D. A. Electrochemical Deposition Regimes and Critical Influence of Organic Additives on the Structure of Bi Films. *J. Alloys Compd.* **2018**, *735*, 1943-1948.

19. Vereecken, P. M.; Rodbell, K.; Ji, C.; Searson, P. C. Electrodeposition of Bismuth Thin Films on n-GaAs (110). *Appl. Phys. Lett.* **2005**, *86*, 121916.

20. Bao, Z. L.; Kavanagh, K. L. Epitaxial Bi/GaAs Diodes via Electrodeposition. *J. Vac. Sci. Technol. B* **2006**, *24*, 2138-2143.

21. Prados, A.; Pérez, L.; Guzmán, A.; Ranchal, R. Mixed Effects of the Atomic Arrangement and Surface Chemistry on the Electrodeposition of Bi Thin Films on n-GaAs Substrates. *J. Phys. Chem. C* **2016,** *120*, 28295–28306.

22. Zhou, L.; Dai, Y.; Zhang, H.; Jia, Y.; Zhang, J.; Li, C. Nucleation and Growth of Bismuth Electrodeposition from Alkaline Electrolyte. *Bull. Korean Chem. Soc.* **2012***, 33*, 1541-1546.

23. Sadale, S. B.; Patil, P. S. Nucleation and Growth of Bismuth Thin Films onto Fluorine-Doped Tin Oxide-Coated Conducting Glass Substrates from Nitrate Solutions. *Solid State Ionics* **2004,** *167*, 273–283.

24. Prados, A.; Ranchal, R.; Pérez, L. Blocking Effect in the Electrodeposition of Bi on n-GaAs in Acidic Electrolytes. *Electrochim. Acta* **2014**, *143*, 23-28.

25. Prados, A.; Ranchal, R.; Pérez, L. Strategies to Unblock the n-GaAs Surface When Electrodepositing Bi from Acidic Solutions. *Electrochim. Acta* **2015**, *174*, 264–272.

26. Lou, X.; Adelmann, C.; Crooker, S. A.; Garlid, E. S.; Zhang, J.; Reddy, K. S. M.; Flexner, S. D.; Palmstrøm, C. J.; Crowell, P. A.; Electrical Detection of Spin Transport in Lateral Ferromagnet-Semiconductor Devices. *Nat. Phys.* **2007**, *3*, 197-202.

27. Yoneyama, H.; Hoflund, G. B. Adsorption on Semiconductor Electrodes. *Prog. Surf. Sci.* **1986**, *21*, 5-92.

28. Palomar-Pardavé, M.; Miranda-Hernández, M.; González, I.; Batina, N. Detailed Characterization of Potentiostatic Current Transients with 2D-2D and 2D-3D Nucleation Transitions. *Surf. Sci.* **1998,** *399*, 80-95.

29. Scharifker, B. R.; Mostany, J. Three-Dimensional Nucleation with Diffusion Controlled Growth. Part I. Number Density of Active Sites and Nucleation Rates per Site. *J. Electroanal. Chem.* **1984,** *177*, 13-23.

30. Hölzle, M. H.; Retter, U.; Kolb, D. M. The Kinetics of Structural Changes in Cu Adlayers on Au(111). *J. Electroanal. Chem. 1***994***, 371*, 101-109.

31. Barrera, E.; Palomar-Pardavé, M.; Batina, N.; González, I. Formation Mechanisms and Characterization of Black and White Cobalt Electrodeposition onto Stainless Steel. *J. Electrochem. Soc.* **2000***, 147*, 1787-1796.

32. Palomar-Pardavé, M.; Aldana-González, J.; Botello, L. E.; Arce-Estrada, E. M.; Ramírez-Silva, M. T.; Mostany, J.; Romero-Romo, M. Influence of Temperature on the Thermodynamics and Kinetics of Cobalt Electrochemical Nucleation and Growth. *Electrochim. Acta* **2017**, *241*, 162-169.

33. Palomar-Pardavé, M.; González, I.; Batina, N.; New Insights into Evaluation of Kinetic Parameters for Potentiostatic Metal Deposition with Underpotential and Overpotential Deposition Processes. *J. Phys. Chem. B* **2000**, *104*, 3545-3555.

34. Licona-Sánchez, T. J.; Álvarez-Romero, G. A.; Mendoza-Huizar, L. H.; Galán-Vidal, C. A.; Palomar-Pardavé, M.; Romero-Romo, M.; Herrera-Hernández, H.; Uruchurtu, J.; Juárez-García, J. M. Nucleation and Growth Kinetics of Electrodeposited Sulfate-Doped Polypyrrole: Determination of the Diffusion Coefficient of SO_4^{2-} in the Polymeric Membrane. *J. Phys. Chem. B* **2010**, *114*, 9737–9743.

35. Hernández-Espejel, A.; Palomar-Pardavé, M.; Cabrera-Sierra, R.; Romero-Romo, M.; Ramírez-Silva, M. T.; Arce-Estrada, E. M. Kinetics and Mechanism of the Electrochemical Formation of Iron Oxidation Products on Steel Immersed in Sour Acid Media. *J. Phys. Chem. B* **2011**, *115,* 1833-1841.

36. Palomar-Pardavé, M.; González, I.; Soto, A. B.; Arce, E. M. Influence of the Coordination Sphere on the Mechanism of Cobalt Nucleation onto Glassy Carbon. *J. Electroanal. Chem.* **1998**, *443*, 125–136.

37. Muñoz, E. C.; Schrebler, R. S.; Cury, P. K.; Suárez, C. A.; Córdova, R. A.; Gómez, C. H.; Marotti, R. E.; Dalchiele, E. A. The Influence of Poly(ethylene oxide) and Illumination on the Copper Electrodeposition Process onto n-Si(100). *J. Phys. Chem. B* **2006**, *110*, 21109-21117.

38. Muñoz, E. C.; Schrebler, R. S.; Córdova, R. A.; Marotti, R. E.; Dalchiele, E. A. Influence of Poly(ethylene oxide) on the Process of Copper Electrodeposition onto p-Si(100). *J. Phys. Chem. C* **2007**, *111*, 16506-16515, 2007.

39. Mayer, T.; Lebedev, M.; Hunger, R.; Jaegermann, W. Elementary Processes at Semiconductor/Electrolyte Interfaces: Perspectives and Limits of Electron Spectroscopy. *Appl. Surf. Sci.* **2005**, *252,* 31-42.

40. Lebedev, M. V.; Masuda, T.; Uosaki, K. Charge Transport at the Interface of n-GaAs (100) With an Aqueous HCl Solution: Electrochemical Impedance Spectroscopy Study. *Semicond.* **2012**, *46*, 471-477.

41. Scharifker, B.; Hills, G. Theoretical and Experimental Studies of Multiple Nucleation. *Electrochim. Acta* **1983**, *28*, 879-889.

42. Rigano, P. M.; Mayer, C.; Chierchie, T. Electrochemical Nucleation and Growth of Copper on Polycrystalline Palladium. *J. Electroanal. Chem. Interfacial Electrochem.* **1988**, *248*, 219-228.

43. Memming, R. *Semiconductor Electrochemistry;* Wiley-VCH: Darmstadt, Germany, 2001. DOI: 10.1002/9783527613069.

44. Sato, N. *Electrochemistry at Metal and Semiconductor Electrodes.* Elsevier Science B.V.: Amsterdam, Netherlands, 1998.

45. Lüth, H. *Surface and Interfaces of Solid Materials;* Springer-Verlag Berlin Heidelberg: Berlin, Germany, 1995.

46. Mönch, W. *Electronic Structure of Metal-Semiconductor Contacts*. Springer: Netherlands, 1990.

47. Oskam, G.; Hoffmann, P. M.; Natarajan, A.; Searson, P. C. *Semiconductor/Electrolyte Boundaries. Wiley Encyclopedia of Electrical and Electronics Engineering;* John Wiley & Sons, Inc.: New York, USA, 2007.

48. Lebedev, M. V.; Mankel, E.; Mayer, T.; Jaegermann, W. Etching of GaAs(100) with Aqueous Ammonia Solution: A Synchrotron-Photoemission Spectroscopy Study. *J. Phys. Chem. C* **2010**, *114*, 21385–21389.

49. Gerischer, H.; Müller, N.; Haas, O. On the Mechanism of Hydrogen Evolution at GaAs Electrodes. *J. Electroanal. Chem.* **1981**, *119*, 41-48.

50. Erné, B. H.; Ozanam, F.; Chazalviel, J. -N. Dynamics of Hydrogen Adsorption on GaAs Electrodes. *Phys. Rev. Lett.* **1998**, *80*, 4337-4340.

51. Sze, S. M. *Physics of Semiconductor Devices*; John Wiley & Sons, Inc.: New York, USA, 1981.

52. Allongue, P.; Souteyrand, E.; Allemand, L. Metal Electrodeposition on Semiconductors. Part III: Description of Charge Transfer for the Formation of Schottky Diodes. *J. Electroanal. Chem.* **1993**, *362*, 89-95.

53. Allongue, P. Steady State Photocapacitance Study of Semiconductor/Electrolyte Junctions II. Surface State Distribution and Charge Transfer Mechanisms. *Ber. Bunsenges. Phys. Chem.* **1988**, *92*, 895-903.

54. Blakemore, J. S. Approximation for Fermi-Dirac Integrals, Especially the Function $F_{1/2}(\eta)$ Used to Describe Electron Density in a Semiconductor. *Solid-State Electron.* **1982**, *25*, 1067-1076.

55. Gerischer, H. The Impact of Semiconductors on the Concepts of Electrochemistry. *Electrochim. Acta* **1990**, *35*, 1677-1699.

56. Arutyunyan, V. M. Physical Properties of the Semiconductor-Electrolyte Interface. *Sov. Phys. Usp.* **1989**, *32*, 521-542.

57. Mendoza-Huizar, L. H.; Robles, J.; Palomar-Pardavé, M. Nucleation and Growth of Cobalt onto Different Substrates Part I. Underpotential Deposition onto a Gold Electrode. *J. Electroanal. Chem.* **2002,** *521,* 95-106.

58. Schröder, K.; Memming, R. Analysis of Trapping and Recombination Effects in Photoelectrochemical Processes at Semiconductor Electrodes: Investigations at n-GaAs. *Ber. Bunsenges. Phys. Chem.* **1985**, *89*, 385-392.

59. Uhlendorf, I.; Reineke-Koch, R.; Memming, R. Analysis of the Hydrogen Formation at GaAs electrodes by Impedance Spectroscopy Investigations. *Ber. Bunsenges. Phys. Chem.* **1995**, *99*, 1082-1090.

60. Erné, B. H.; Stchakovsky, M.; Ozanam, F.; Chazalviel, J. N. Surface Composition of n-GaAs Cathodes during Hydrogen Evolution Characterized by In Situ Ultraviolet-Visible Ellipsometry and In Situ Infrared Spectroscopy. *J. Electrochem. Soc.* **1998,** *145*, 447-456.

61. Padovani, F. A.; Stratton, R. Field and Thermionic-Field Emission in Schottky Barriers. *Solid-State Electron.* **1966**, *9*, 695-707.

62. Palomar-Pardavé, M.; Scharifker, B.; Arce, E. M.; Romero-Romo, M. Nucleation and Diffusion-Controlled Growth of Electroactive Centers. Reduction of Protons During Cobalt Electrodeposition**.** *Electrochim. Acta* **2005,** *50*, 4736-4745.

63. Fleischmann, M.; Thirsk, H. R. The Potentiostatic Study of the Growth of Deposits on Electrodes. *Electrochim. Acta* **1959,** *1*, 146-160.

64. Scharifker, B. R.; Mostany, J.; Palomar-Pardavé, M.; González, I. On the Theory of the Potentiostatic Current Transient for Diffusion-Controlled Three-Dimensional Electrocrystallization Processes. *J. Electrochem. Soc.* **1999**, *146*, 1005-1012.

65. Vereecken, P. M.; Searson, P. C. Electrochemical Deposition of Bi on GaAs (100). *J. Electrochem. Soc.* **2001**, *148*, C733-C739.

66. Härk, E.; Lust, K.; Lust, E. Electrochemical Impedance Study of Hydrogen Evolution on Bi(001) Electrode in the $HClO_4$ Aqueous Solutions. *J. Solid State Electrochem.* **2009**, *13*, 745–754.

67. Lust, K.; Perkson, E.; Lust, E. Kinetics of Hydrogen Evolution on Single Crystal Bismuth Electrodes. *Russ. J. Electrochem.* **2000,** *36*, 1257-1262.

68. Trassati, S. Work Function, Electronegativity, and Electrochemical Behaviour of Metals. III. Electrolytic Hydrogen Evolution in Acid Solutions. *J. Electroanal. Chem. Interfacial Electrochem.* **1972**, *39*, 163-184.

69. Sebastián, P.; Botello, L. E.; Vallés, E.; Gómez, E.; Palomar-Pardavé, M.; Scharifker, B. R.; Mostany, J. Three-Dimensional Nucleation with Diffusion Controlled Growth: A Comparative Study of Electrochemical Phase Formation from Aqueous and Deep Eutectic Solvents. *J. Electroanal. Chem.* **2017**, *793*, 119-125.

70. Le Manh, T.; Arce-Estrada, E. M.; Romero-Romo, M.; Mejía-Caballero, I.; Aldana-González, J.; Palomar-Pardavé, M. On Wetting Angles and Nucleation Energies during the Electrochemical

Nucleation of Cobalt onto Glassy Carbon from a Deep Eutectic Solvent. *J. Electrochem. Soc.* **2017**, *164*, D694-D699.

71. Cadle, S. H.; Bruckenstein, S. Ring-Disk Electrode Study of the Reduction of Bismuth on Platinum. *Anal. Chem.* **1972**, *44*, 1993-2001.

72. Depestel, L. M.; Strubbe, K. Influence of the Crystal Orientation on the Electrochemical Behaviour of n-GaAs in Au(I)-Containing Solutions. *Phys. Chem. Chem. Phys.* **2003**, *5*, 2881-2885.

73. Barradas, R. G.; Bosco, E. A Kinetic Model of Multilayer Adsorption in Electrochemical Phase Formation. *J. Electroanal. Chem. Interfacial Electrochem.* **1985**, *193*, 23-26.

74. Erné, B. H.; Ozanam, F.; Chazalviel, J. -N. The Mechanism of Hydrogen Gas Evolution on GaAs Cathodes Elucidated by In Situ Infrared Spectroscopy. *J. Phys. Chem. B* **1999**, *103*, 2948-2962.

TOC Graphic